Linear-Quadratic-Gaussian Torque Control:
Application to a Flexible Joint of a Rehabilitation Exoskeleton

R.Vertechy, A. Frisoli, M. Solazzi, A. Dettori and M. Bergamasco

Abstract—**A linear-quadratic-Gaussian regulator is proposed for the torque control of flexible robotic joints with built-in torque sensor. The regulator requires the joint-torque sensor information only and features: 1) a Kalman filter that, beside reducing the noise and evaluating the derivative of the torque sensor measure, is able to estimate all the external and internal torques acting on the joint; 2) a controller that optimizes system stability, responsiveness, accuracy and effort. The regulator is implemented on a flexible joint of a rehabilitation exoskeleton. Simulation and experimental results are provided which demonstrate regulator performance and efficacy.**

I. INTRODUCTION

THE reduction in motor functionality of upper extremities is one of the most common impairments resulting from spinal cord injuries, occupational and sport accidents, strokes and other disease processes. In these cases, partial or full sensorimotor recovery can be achieved trough intense and constant rehabilitation protocols based on active and highly repetitive exercises [1, 2]. In the last decade, Robotic Assisted (RA) and Virtual Reality Based (VRB) rehabilitation have been proposed [3] for improving treatment outcomes, mitigating therapists' workload and reducing overall healthcare expenses (for both patient and providers). Pilot studies demonstrated that RA and VRB rehabilitation are more effective for the recovery of upper limb function as compared to usual manual therapies [4-6].

On the basis of the experience gained at PERCRO laboratory during the clinical evaluation [6] of the L-EXOS [7] in the rehabilitation of stroke patients, a novel exoskeleton prototype, hereafter called RehabExos, has been conceived for the rehabilitation of upper extremities [8]. The RehabExos (shown in Fig. 1) has a serial architecture that is isomorphic with the human kinematics and comprises: a shoulder joint which is fixed in space and composed by three active joints J1, J2 and J3; an active elbow joint J4; and a passive revolute joint J5 allowing for wrist pron-/supin-ation. The RehabExos is aimed at generating controlled contact forces not only at the exoskeleton end-

link handle, but also at some intermediate link. This makes it possible to apply forces to selected joints or limbs of the patient upper extremity (e.g. arm, forearm, shoulder, elbow and wrist) and to modulate their magnitude depending on patient deficiency and exercise type.
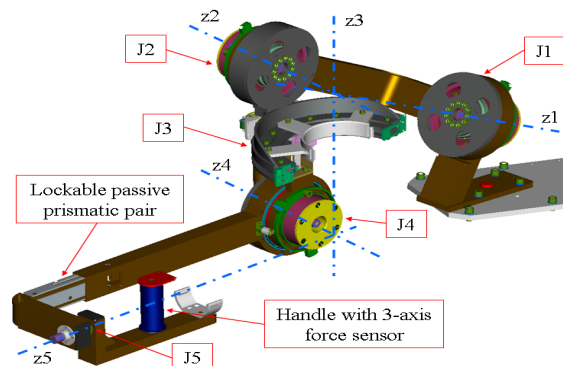

Fig. 1. General kinematics of the RehabExos

For this purpose, the patient can be constrained to the RehabExos links at the level of his/her hand, arm and forearm. Other RehabExos features are: exercisable force at the end-effector of 100N (in every direction and in each point of the workspace); back-drivability of the system at motor power-off for safety and good transparency at motor power-on; possibility of easily changing configuration for the right and left extremity; modular design for affordability and maintenance ease. Actuation of the RehabExos is provided in loco via identical custom made actuation groups (hereafter indicated with AG1) for J1, J2 and J4, and via a different custom made actuation group (hereafter indicated with AG2) for J3. Both AG1 and AG2 comprise an electric motor, a geared transmission with rather large reduction ratio (which optimizes the actuation group torque-to-weight performance) and unavoidable compliance, a motor-side rotary encoder and a joint-torque sensor. For a more detailed description of both RehabExos and actuation groups please refer to [8].

Internal joint-torque sensors have been included in AG1 and AG2 in order to enhance overall exoskeleton control. Indeed, although augmenting the group compliance, the availability of such a sensor enables: closing a stable high-bandwidth torque inner loop around the joint which is scarcely affected by the robot link variable inertia [9, 10]; suppressing the robot vibrations produced by the inherent transmission compliance [11-13]; reducing internal

disturbance torques caused by actuator and reducer (for instance friction losses, actuator torque ripples and gear teeth wedging actions [14]); measuring externally applied forces/moments and complex nonlinear dynamic interactions between the joint and the other robot links [15]. Owing to the significant compliance of both mechanical transmission and internal joint-torque sensor, AG1 and AG2 must be regarded as flexible robotic joints.
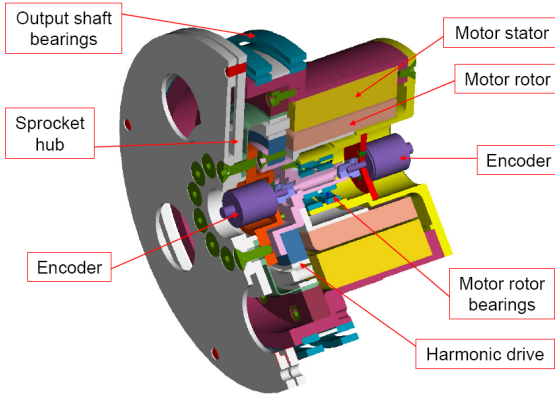

Fig. 2. CAD section exploded view of the Actuation Group 1 (AG1) with the indication of the principal elements

In this context, the present work deals with the joint-torque control of AG1. The problem of controlling the output torque of flexible robotic joints has been addressed extensively in the literature. For instance: proportional or Proportional-Derivative (PD) Joint-Torque-Feedback (JTF) laws, eventually integrating compensators for internal motor disturbance, which are based on either feed-forward models or minimum order observers, have been proposed in [16-20]; an acceleration-controller-based torque regulator integrating a compensator for the internal motor disturbances, which is based on a minimum order observer, is proposed in [21]; a H_∞ torque control based on empirical system models obtained through experimental frequency response estimates is proposed in [22]. Here, by resorting to a state-space approach, a novel Linear-Quadratic-Gaussian (LQG) JTF regulator is presented. It features a PD JTF law that integrates a compensator for all the internal and external forces/torques acting on the system (and not for the internal motor disturbances only). The regulator gains are selected by ensuring system stability and compromising between system responsiveness, accuracy and motor effort. The regulator comprises also a Kalman filter which: 1) makes it possible to clean optimally the torque sensor measurement from the significant noise that is induced by the electronic switching of the motor driver and that usually degrades JTF controller performances; 2) by making use of a mathematical artifice based on the properties of the stochastic Wiener process, is also capable of estimating all the internal and external forces/torques acting on the flexible joint. All these features are not offered by currently available JTF schemes.

The proposed LQG regulator is employed for the torque control of AG1. Both simulation and experimental results are presented which show both the efficacy of the proposed regulator and the major differences with respect to the most popular JFT controllers.
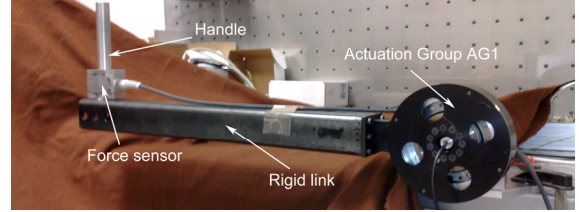

Fig. 3. Manufactured prototype of the Actuation Group 1 (AG1) and its test-rig.

I. THE ACTUATION GROUP AG1

As described, the three DOF of the RehabExos that are provided by joints J1, J2 and J4 are motorized through identical actuation groups identified as AG1. A dissected CAD view of AG1 is reported in Fig. 2. It consists of a custom-made frameless brushless torque motor integrating a very compact Harmonic Drive (HD) component set (its axial length is 50% of that of standard HDs), two redundant optical encoders, two thin output shaft bearings, and a torque sensor consisting of two fully balanced strain gauge bridges placed on different beams of a thin planar sprocket hub. The sprocket hub is connected to the HD output at one side and to the AG1 output shaft at the other. Such an architecture makes the torque sensor insensitive to non-torsional components of the external loads acting on the output shaft. Despite the joint torque could have been measured by placing the strain gauges directly on the HD flexspline [23], here the addition of a sprocket hub has been preferred since the chosen HD is a very compact one, thus it is very difficult to instrument, and since HD-based torque sensing inherently introduce significant measurement errors (modulation errors) which require large numbers of strain gauges and appropriate filtering techniques for compensation [24, 25]. The sprocket hub is made of steel (AISI 630), while the motor housing and the non-commercial components are made of aluminium alloy (Ergal 7075 T6). The specifications and practical performance of AG1 are: transmission reduction ratio equal to 100; motor rotor maximum velocity equal to 1000rpm; encoders pulses-to-revolution equal to 5000; nominal motor stall torque equal to 2Nm (motor side); limiting average joint output torque equal to 150Nm (joint output side); joint-torque sensor measurement range equal to ±120Nm (sprocket hub deformation is limited by mechanical stops); torque sensor variance W = 0.12Nm (measured with the motor driver turned on); overall weight equal to 3.7Kg; motor shaft inertia reduced to the joint output shaft J_m = 2.5Kgm^2; overall joint torsional stiffness reduced to the joint output shaft k = 6.3kNm/rad. Owing to the adopted mechanical components, AG1 features limited joint back-drivability at motor power-off and limited mechanical complexity to ease maintenance as well as cost reduction.

For the sake of this work, an AG1 prototype is embedded in a test-rig. As shown in Fig. 3, such a test-rig consists of a fixed frame attached to the motor stator, a rigid link attached to the AG1 output shaft, and a handle. The rigid link inertia (reduced to the joint output shaft) is $J_l = 0.7 \text{Kgm}^2$. The handle has a single axis force sensor, which enables direct measurement of the external forces a user can exchange with the link (here, this sensor is not used for torque control but only for evaluation purposes).
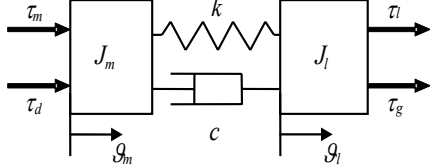

Fig. 4. Lumped parameter model of the flexible joint

II. FLEXIBLE JOINT MODEL

The design of a torque controller for the flexible joint shown in Fig. 3 requires an adequate model of the system dynamics. A lumped parameter model is given in Fig. 4. In the model, J_m and J_l are the overall moments of inertia of the elements which are fixed with respect to motor rotor and joint output link, ϑ_m and ϑ_l are the angular positions of motor rotor and joint output link, τ_m and τ_d are the internal commanded and disturbance (which accounts for friction and ripple effects of both motor and harmonic drive) torques acting directly on the motor rotor, τ_g and τ_l are the external torques acting directly on the joint output link which are due to the gravitational field and to the contact interaction with the environment (for instance with a human user), k and c are the overall stiffness and damping coefficients of the flexible joint (principally due to the harmonic drive and the torque sensor). Owing to the presence of a mechanical transmission (i.e. the harmonic drive), note that all the aforementioned quantities are considered as being reduced to the same moving shaft, for instance the joint output link.

The dynamics of the system depicted in Fig. 4 is governed by the following equations

$$\begin{cases} J_m \ddot{\vartheta}_m = \tau_m + \tau_d + k\left(\vartheta_l - \vartheta_m\right) + c\left(\dot{\vartheta}_l - \dot{\vartheta}_m\right) \\ J_l \ddot{\vartheta}_l = \tau_l + \tau_g - k\left(\vartheta_l - \vartheta_m\right) - c\left(\dot{\vartheta}_l - \dot{\vartheta}_m\right) \end{cases} \quad (1)$$

Assuming that the flexible joint is equipped with an internal torque sensor capable of measuring the elastic torque τ_s (hereafter called sensor torque), which acts between motor rotor and joint output link, i.e. $\tau_s = k\ (\vartheta_l - \vartheta_m)$, and by considering its time derivatives, the sensor torque dynamics reads as

$$\ddot{\tau}_s + \frac{c}{J}\dot{\tau}_s + \frac{k}{J}\tau_s = \frac{k}{J_l}\tau_l + \frac{k}{J_l}\tau_g - \frac{k}{J_m}\tau_d - \frac{k}{J_m}\tau_m \quad (2)$$

where $J = [J_m J_l / (J_m + J_l)]$. With reference to the test-rig depicted in Fig. 3, the spectrum of the joint sensor torque τ_s

in response to the motor torque command τ_m (both reduced to the output shaft of AG1) is reported in Fig. 5. This Bode magnitude plot is obtained experimentally by commanding τ_m with a chirp function. As (2) predicts, the test-rig possesses a marked natural frequency at $\sqrt{k/J}/2\pi \approx 17 \text{Hz}$. From Fig. 4, use of the Half-Power Bandwidth method returns $c = 11.8 \text{Nms/rad}$ as the overall damping coefficient of the flexible joint (this value has also been validated via the Logarithmic Decrement method).
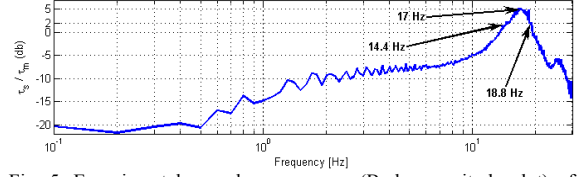

Fig. 5. Experimental open-loop response (Bode magnitude plot) of AG1: joint sensor torque *vs.* motor torque command

III. FLEXIBLE JOINT AND JOINT TORQUE FEEDBACK CONTROL

Environment interacting robots, in particular haptic and rehabilitation devices, are machines which modulate the forces/torques they exchange with the surroundings, in particular the human user. Referring to the one-degree-of-freedom flexible joint schematized in Fig. 4, this reduces to the regulation of τ_l by the action on τ_m. Equation (2) highlights that while the dynamics of the sensor torque τ_s can be shaped as desired by designing a proper feedback law for the commanded motor torque τ_m, conversely the external torque τ_l is not controllable via τ_m. Besides, the availability of a stable, fast and accurate torque control loop on τ_s (i.e. a JTF control) can enhance enormously the adjustment of the external torque τ_l. Indeed, by forcing $\tau_s \approx \tau_s^D$ and $\dot{\tau}_s \approx 0$, where τ_s^D is a desired sufficiently smooth-varying sensor torque, the second equation of (1) tends to $J_l \ddot{\vartheta}_l \approx \tau_l + \tau_g - \tau_s^D$, which reduces the dynamics of the flexible joint to that of a direct drive system having the desired torque τ_s^D as command (see Fig. 6). Then, the design of τ_s^D as a well-behaved function of ϑ_l (along with its time derivatives) and of τ_g (which can be easily calculated as a function of ϑ_l) enables the regulation of the interaction torque τ_l as well as the contact impedance of the joint output link. For instance, if the angular acceleration of the output link is available (via either direct measurement or an estimator), the adoption of a stable fast and accurate JTF control with $\tau_s^D \approx (\tau_l^D + \tau_g - J_l \ddot{\vartheta}_l)$ can be used to force $\tau_l \approx \tau_l^D$, where τ_l^D is the desired joint output link torque. In addition, whenever a direct measurement of τ_l is available, a similar result (i.e. $\tau_l \approx \tau_l^D$) can be obtained by setting the JTF control with $\tau_s^D = [\tau_l^D + \tau_g + k_{\tau l}(\tau_l^D - \tau_l)]$, where $k_{\tau l}$ is an appropriate feedback error gain of an outer torque loop. Note that for most haptic applications, and in particular for rehabilitation, which usually involve motions with rather limited accelerations, the simple choice $\tau_s^D = (\tau_l^D + \tau_g)$
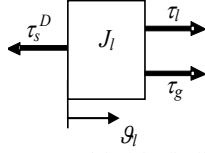
suffices.

Fig. 6. Lumped parameter model of the flexible joint with JTF control

IV. FLEXIBLE JOINT STATE-SPACE CONTROLLER

In this section, the design of a stable JTF controller that is capable of tracking $\tau_s \approx \tau_s^D$ and $\dot{\tau}_s \approx 0$ with great accuracy and responsiveness is performed via a state-space approach [26]. For the purpose of JTF control, (2) is recast in the following state-space system

$$\dot{e} = \mathbf{A}e + \mathbf{B}\tau_m + \mathbf{E}\tau_0 \qquad (3.1)$$

where τ_m is the control input,

$$e = \begin{bmatrix} \tau_s - \tau_s^D \\ \dot{\tau}_s \end{bmatrix}, \quad \tau_0 = \begin{bmatrix} \tau_{lgd} \\ \tau_s^D \end{bmatrix}, \quad \dot{\tau}_0 = \mathbf{0} \qquad (3.2)$$

are the controllable and the uncontrollable (i.e. exogenous input) variables, $\tau_{lgd} = [\tau_l + \tau_g - \tau_d (J_l / J_m)]$, and

$$\mathbf{A} = \begin{bmatrix} 0 & 1 \\ -k/J & -c/J \end{bmatrix}, \mathbf{B} = \begin{bmatrix} 0 \\ -k/J_m \end{bmatrix}, \mathbf{E} = \begin{bmatrix} 0 & 0 \\ k/J_l & -k/J \end{bmatrix} \quad (3.3)$$

Note that (3) assumes $\dot{\tau}_s^D \approx 0$ (i.e. τ_s^D is a sufficiently smooth-varying desired sensor torque). For more demanding applications, whenever $\dot{\tau}_s^D$ is available, the controllable variable $\dot{e} = \dot{\tau}_s$ can be replaced by $\dot{e} = \dot{\tau}_s - \dot{\tau}_s^D$ whilst $\mathbf{E}$ and τ_0 augmented to account $\dot{\tau}_s^D$ as supplementary exogenous input variable. According to (3), the following full-state feedback law is obtained

$$\tau_m = \tau_{m,1} = -\left[k_1 \left(\hat{\tau}_s - \tau_s^D \right) + k_2 \hat{\dot{\tau}}_s + k_3 \hat{\tau}_{lgd} + k_4 \tau_s^D \right] \qquad (4)$$

where k_1, k_2, k_3 and k_4 are the controller gains, while $\hat{\tau}_s$, $\hat{\dot{\tau}}_s$, $\hat{\tau}_{lgd}$ and τ_s^D are the estimates of both controllable and exogenous state-space variables. Note that whenever a reliable model $\hat{\tau}_d$ is readily available for the motor disturbance τ_d, (4) can be replaced by

$$\tau_m = \tau_{m,2} = -\left[k_1 \left(\hat{\tau}_s - \tau_s^D \right) + k_2 \hat{\dot{\tau}}_s + k_3 \hat{\tau}_{lg} + k_4 \tau_s^D \right] - \hat{\tau}_d \quad (5)$$

where $\hat{\tau}_{lg}$ is the estimate of the overall external torque $\tau_{lg} = (\tau_l + \tau_g)$, which acts on the joint output link only.

In principle, the appropriate choice of the controller gains makes it possible to shape at will the dynamic response of τ_s to τ_s^D. In order to mediate between the exigencies of fast and accurate system response and the saturation limits of the control command τ_m, the gains k_1, k_2, k_3 and k_4 are selected in the framework of Linear-Quadratic (LQ) optimum control [26]. In particular, k_1, k_2, k_3 and k_4 are chosen as the steady-state gains that minimize the following performance integral

$$LQ = \int_t^T \left[q_1^2 \left(\tau_s - \tau_s^D \right)^2 + q_2^2 \dot{\tau}_s^2 + \tau_m^2 \right] \cdot dt \qquad (6)$$

where q_1 and q_2 are penalty parameters relative to the cost of control. As for their physical significance, the choice of q_1 influences directly the system tracking error e (i.e. larger q_1 leads to smaller e), while the choice of the ratio q_2/q_1 influences directly system stability and responsiveness (i.e. rising q_2/q_1 increases stability and reduces time-response). Augmenting q_1 and q_2 enlarges controller effort. The practical mathematical procedure for calculating k_1, k_2, k_3 and k_4 for a given system (i.e. equations (4) and (6)) and chosen penalty parameters is detailed in [26].

As compared to the most popular JTF laws, the controller described by either (4) or (5) (hereafter called JTF1) differs from that described in [17, 18] (hereafter called JTF2) since there $k_3 = 0$ and $k_4 = (1 + J_m/J_l)$, and from that described in [19, 20] (hereafter called JTF3) since there $k_3 = 0$ and $k_4 = 1$. That is, the controller proposed here can be considered as a generalization of those given in [17-20].

V. FLEXIBLE JOINT OPTIMUM OBSERVER

Beside the availability of τ_s^D, the JTF control scheme proposed in the previous section requires the knowledge of the state-space variable estimates $\hat{\tau}_s$, $\hat{\dot{\tau}}_s$ and $\hat{\tau}_{lgd}$ (or $\hat{\tau}_{lg}$ and $\hat{\tau}_d$ if (5) is used instead of (4)). Here, a Kalman filter (optimum observer [26]) is proposed to infer $\hat{\tau}_s$, $\hat{\dot{\tau}}_s$ and $\hat{\tau}_{lgd}$ from a single noisy measurement τ_s^m, $\tau_s^m = (\tau_s + w)$, where w is the noise affecting the torque sensor embedded in the flexible joint (the major contribution to w is usually the electrical noise excited by the motor driver switching electronics). For the purpose of variable estimation (both controllable states and exogenous input), the dynamics governed by (2) and (4) can be described by the following meta-system

$$\begin{cases} \dot{\tau} = \mathbf{A}'\tau + \mathbf{B}'\tau_{m,1} + \boldsymbol{\Gamma}v \\ y = \tau_s^m = \mathbf{C}\tau + w \end{cases} \qquad (7.1)$$

where $\tau^T = [\tau_s \ \dot{\tau}_s \ \tau_{lgd}]$ is the meta-state vector, w and v are white noise processes with known variances W and V, $\mathbf{C} = [1 \ 0 \ 0]$ and

$$\mathbf{A}' = \begin{bmatrix} 0 & 1 & 0 \\ -k/J & -c/J & k/J_l \\ 0 & 0 & 0 \end{bmatrix}, \mathbf{B}' = \begin{bmatrix} 0 \\ -k/J_m \\ 0 \end{bmatrix}, \boldsymbol{\Gamma} = \begin{bmatrix} 0 \\ 0 \\ 1 \end{bmatrix} \quad (7.2)$$

Note that in order for the Kalman filter to estimate the

exogenous input τ_{lgd}, the dynamics of such an unknown variable is assumed as the Wiener process (i.e. a non stationary random process) $\dot{\tau}_{lgd} = v$, which, in practice, only forces τ_{lgd} to be continuous and varying with independent increments. According to (7), the following optimum observer is obtained

$$\dot{\hat{\boldsymbol{\tau}}} = \mathbf{A}'\hat{\boldsymbol{\tau}} + \boldsymbol{B}'\tau_{m,1} + \boldsymbol{L}\left(y - \boldsymbol{C}\hat{\boldsymbol{\tau}}\right) \qquad (8)$$

where $\hat{\boldsymbol{\tau}}^T = [\hat{\tau}_s \quad \hat{\dot{\tau}}_s \quad \hat{\tau}_{lgd}]$ is the meta-state vector estimate and $\boldsymbol{L}$ is the steady-state Kalman gain vector. The practical mathematical procedure for calculating $\boldsymbol{L}$ for a given system (i.e. once (7) is known) and noise process variances (i.e. W and V) is detailed in [26]. In this regard, note that the variance W is evaluated directly from the torque sensor measure, while the ratio V/W is chosen so that to compromise between estimator accuracy and precision (i.e. larger V/W leads to more accurate but less precise estimates).

It is worth to mention that when a reliable model $\hat{\tau}_d$ is readily available for the motor disturbance τ_d, such that (5) is used instead of (4) for JTF control, the substitution in (8) of $\tau_{m,1}$ with $(\tau_{m,2} + \hat{\tau}_d)$ enables to find $\hat{\tau}_{lg}$ instead of $\hat{\tau}_{lgd}$.

It is worth to mention that the JTF implementations, which can be found in the literature for the torque control of flexible joints, do not consider the possibility of reconstructing the exogenous variable τ_{lgd} (or τ_{lg} if (5) is used instead of (4)) from the measurement of the built-in joint-torque sensor. Indeed, just minimum order observers for the estimation of τ_d only have been devised and employed which require the additional measurement of either motor position ϑ_m [18, 21, 27, 28] or motor velocity $\dot{\vartheta}_m$ [13]. Moreover, in these JTF implementations, the estimates $\hat{\tau}_s$ and $\hat{\dot{\tau}}_s$ are obtained by simply feeding the torque sensor measurement y through basic low-pass and derivative filters, instead of reconstructing them via the optimal observer given by (8). This may degrade JTF control performance since built-in joint-torque sensors are usually affected by noise w having significant variance.

VI. SIMULATION AND EXPERIMENTAL RESULTS

The combination of (4) (or (5)) with (8) gives a LQG torque regulator for flexible robotic joints. In this section, such a regulator is employed for the control of the system depicted in Fig. 3. According to the system properties already described in Section II, the choice $V = 10^4$ yields the following Kalman gain vector $\boldsymbol{L} = [199, 19854, 289]^T$, whereas the choice $q_1 = 500$ and $q_2 = 0.1$ gives the controller gains $k_1 = -18.3$, $k_2 = -0.33$, $k_3 = -2.81$ and $k_4 = 3.62$.

The synthesized controller is first tested in simulation to verify the performance of the proposed novel control law JTF1 with respect to the existing JTF2 [17, 18] and JTF3 [19, 20]. In the simulation, the following working conditions
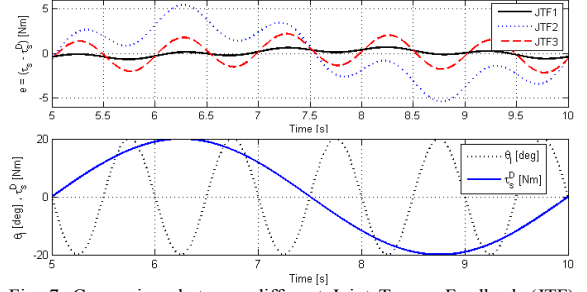

Fig. 7. Comparison between different Joint Torque Feedback (JTF) laws (simulation results)

are considered: $\tau_d = \tau_g = W = 0$, $\tau_s^D = [20 \sin(0.4\pi t)]$Nm ($t$ being the elapsed time), $\vartheta_l = [20 \sin(2\pi t)]$deg (that is, the controller attempts to track τ_s^D while the output link is moved according to a given trajectory; measurement errors are not considered here). Simulation results are reported in Fig. 7, which highlights the better performance (i.e. smaller tracking error e, see upper plot) of JTF1 with respect to both JTF2 and JTF3. In particular the tracking error obtained with JTF1 is $|e| \leq 0.3$Nm.
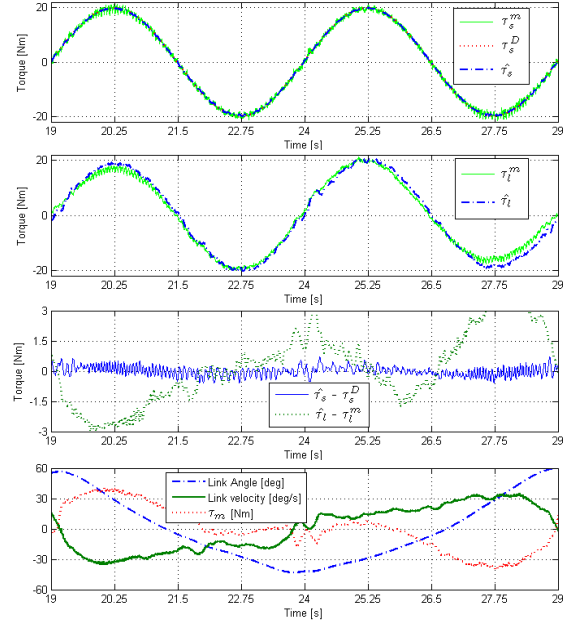

Fig. 8. Performance of the proposed Linear-Quadratic-Gaussian (LQG) torque regulator (experimental results)

Then, the proposed LQG regulator is assessed on the test-rig shown in Fig. 3. In the experiment, the joint axis is vertical so that $\tau_g = 0$. Moreover, disposing of the experimentally determined [8] motor friction torque model $\hat{\tau}_d = [-13.7 \cdot \text{sign}(\dot{\vartheta}_m)(1 + \tanh(|\dot{\vartheta}_m / 2| - 4)) / 2]$ Nm, the controller implements (5) instead of (4). Since $\tau_g = 0$, the Kalman filter makes it possible to get an estimate of the external torque τ_l (i.e. $\hat{\tau}_l$). In the experiment, the following desired torque is considered $\tau_s^D = [20 \sin(0.4\pi t)]$Nm, while the end link is moved in the range $\vartheta_l \in [-60,60]$deg by a human user who acts on the sensorized handle of the test-rig

(see Fig. 3). Experimental results are reported in Fig. 8, which highlights (third plot from the top) that the proposed controller is able to keep the torque sensor tracking error e within ± 0.5Nm (which is about the same value as that obtained in simulation and of the noise of the joint-torque sensor measure). The effectiveness of the Kalman filter in the estimation of τ_s and τ_l is shown, respectively, in the first two diagrams where the estimates $\hat{\tau}_s$ and $\hat{\tau}_l$ are plotted over the raw measurements τ_s^m and τ_l^m (τ_l^m being measured via the force sensor placed at the test-rig handle). The significant difference (roughly ± 3Nm) between $\hat{\tau}_l$ and τ_l^m, which is also evidenced in the third plot from the top, is only due to the imperfection of the adopted friction model $\hat{\tau}_d$ (in practice, $\hat{\tau}_l$ depends on τ_l^m but also on the error between the real and the modeled motor disturbance torque). The bottom graph plots the position and velocity of the output link along with the commanded motor torque τ_m. As shown, τ_m is rather smooth and remains within ± 40Nm and does not exceed too much the maximum of the sum of desired sensor torque and motor friction torque (i.e. $\max(\tau_s^D + \hat{\tau}_d) \approx 33.7$ Nm).

VII. CONCLUSION

This paper have proposed and demonstrated, both in simulation and through experiments, Linear-quadratic-Gaussian control for the torque regulation of flexible robotic joints with built-in torque sensor. As compared to other available joint-torque-feedback controllers, the proposed method makes it possible to overcome most of the issues related to the presence of noise in the joint-torque sensor measure and to the lack of knowledge of both external and internal torques acting on the joint. Controller tuning is very simple and amounts to the selection of two parameters that directly relate to the stability, responsiveness and accuracy of the system, and to the controller effort.

REFERENCES

[1] H.M. Feys, W.J. De Weerdt, B.E. Selz, G.A. Cox Steck, R. Spichiger, L.E. Vereeck, K.D. Putman, G.A. Van Hoydonck. Effect of a Therapeutic Intervention for the Hemiplegic Upper Limb in the Acute Phase After Stroke: A Single-Blind, Randomized, Controlled Multicenter Trial. Stroke, vol. 29, pp. 785-792, 1998.

[2] L. Diller. Post-stroke rehabilitation practice guidelines. International handbook of neuropsychological rehabilitation. Critical issues in neurorehabilitation, New York: Plenum, pages 167–82, 2000.

[3] HI Krebs, N. Hogan, ML Aisen, and BT Volpe. Robot-aided neurorehabilitation. IEEE Transactions on Rehabilitation Engineering, vol. 6(1), pp. 75–87, 1998.

[4] D.J. Reinkensmeyer, L.E. Kahn, M. Averbuch, A. McKenna-Cole, B.D. Schmit, W.Z. Rymer. Understanding and treating arm movement impairment after chronic brain injury: Progress with Arm Guide. Journal of Rehabilitation Research and Development, 37(6), 2000.

[5] J. Stewart, S. Yeh, Y. Jung, H. Yoon, M. Whitford, S. Chen, L. Li, M. McLaughlin, A. Rizzo, C. Winstein. Pilot Trial Results from A Virtual Reality System Designed to Enhance Recovery of Skilled Arm and Hand Movements after Stroke. International Workshop on Virtual Rehabilitation, pp. 18-23, 2006.

[6] A. Frisoli, A. Montagner, L. Borelli, F. Salsedo, M. Bergamasco. A force-feedback exoskeleton for upper limb rehabilitation in Virtual Reality. Applied Bionics and Biomechanics Vol. 00, No. 00, December 2008, 1-17.

[7] F. Salsedo, A. Dettori, A. Frisoli, F. Rocchi, M. Bergamasco, M. Franceschini. Exoskeleton Interface Apparatus. 2002.

[8] R. Vertechy, A. Frisoli, A. Dettori, M. Solazzi, M. Bergamasco. Development of a new exoskeleton for upper limb rehabilitation. Proc. IEEE Int. Conf. on Rehabilitation Robotics, pp. 188-193, 2009.

[9] J. Luh, W. Fisher, R. Paul. Joint Torque Control by a Direct Feedback for Industrial Robots. IEEE Trans. Automan. Contr., vol. AC-28, n. 2, pp153-161, 1983.

[10] C.H. An, J.M. Hollerbach. Dynamic Stability Issues in Force Control of Manipulators. Proc. IEEE Int. Conf. Robotics Automat, pp. 890-896, Rayleg, US, 1983.

[11] M. Hashimoto. Robot Motion Control Based on Joint Torque Sensing. Proc. IEEE International Conference Robotics and Automation, vol. 1, pp. 256-261, Scottsdale, 1989.

[12] S.D. Eppinger and W.P. Seering. Understanding Band width Limitations in Robot Force Control. Proc. IEEE Int. Conf. Robotics and Automantion, pp. 904-909, Raylegh, US, 1987.

[13] G. Zhang, J. Furusho. Control of Robot Arms Using Joint Torque Sensors. Proc. of IEEE Int. Conf. on Robotics and Automation, pp. 3148-3153, New Mexico, 1997.

[14] L.E. Pfeffer, O. Khatib, J. Hake. Joint Torque Sensory Feedback in the Control of the PUMA Manipulator. IEEE Trans. Robotics and Automation, vol 5, n. 4, pp.418-425, 1989.

[15] K. Kosuge, H. Takeuchi, K. Furuta. Motion Control of a Robot Arm Using Joint Torque Sensors. Proc. 27th Conf. Decision Control, Austin, US, 1988.

[16] C.H. Wu, R.P. Paul. Manipulator Compliance Based on Joint Torque Control. Proc. IEEE Conf. Decision Contr., vol. 1, pp. 88-94, Albuquerque, 1980.

[17] M. Hashimoto, Y. Kiyosawa, R.P. Paul. A Torque Sensing Technique for Robots with Harmonic Drives. IEEE Transactions on Robotics and Automation, vol. 9, n. 1, pp. 108-116, 1993.

[18] M. Hashimoto, Y. Kiyosawa. Expermental Study on Torque Control Using Harmonic Drive Built-in Torque Sensors. Journal of Robotic Systems, vol. 15, n. 8, pp. 435-445, 1998.

[19] A. Albu-Shaffer, G. Hirzinger. State Feedback controller for flexible joint robots: A globally stable approach implemented on DLR's light-weight robots. Proc of 2000 IEEE/RSJ Int. Conf. on Intelligent Robots and Systems, pp. 1087-1093, Takamatsu, Japan, 2000.

[20] C. Ott, A. Albu-Shaffer, A. Kugi, G. Hirzinger. On the Passivity Based Impedance Control of Flexible Joint Robots. IEEE Transaction on Robotics, vol. 24, n. 2, pp. 416-429, 2008.

[21] K. Kaneko, T. Murakami, K. Ohnishi, K. Komoriya. Torque Control with Nonlinear Compensation for Harmonic Drive DC Motors. 20th International Conference on Industrial Electronics, Control and Instrumentation, vol. 2, pp. 1022-1027, Bologna, Italy, 1994.

[22] H.D. Taghirad, P.R. Belanger. H∞ Based Robust Torque Control of Harmonic Drive Systems Under Free- and Constrained-Motion Applications. Proc. IEEE Int. Conf. on Control Applications, pp. 990-994, Trieste, Italia, 1998.

[23] M. Hashimoto. Robot motion control based on joint torque sensing. International Conference on Robotics and Automation 1989, vol.1, pp. 256-261, Scottsdale, AZ, 14-19 May 1989.

[24] I. Godler, M. Hashimoto. Torque control of harmonic drive gears with built-in sensing. IECON '98, Proceedings of the 24th Annual Conference of the IEEE Industrial Electronics Society, vol. 3, pp. 1818-1823, Aachen, Germany, 1998.

[25] H. D. Taghirad, A. Helmy, P. R. B'elanger. Intelligent built-in torque sensor for harmonic drive system. IEEE Transaction on Instrumentation and Measurement, vol. 48, n. 6, 1999.

[26] B. Friedland. Control System Design: An Introduction to State Space Methods, Dover Publications, New York, 2005.

[27] K. Kaneko, N. Suzuki, K. Ohnishi, K. Tanie. High Stiffness Torque Control for Geared DC Motor Based on Acceleration Controller. Proc. of IEEE Int. Conf. on Industrial Electronics Instrumentation and Control, pp. 849-854, Kobe, Japan, 1991.

[28] K. Kaneko, K. Komoriya, K. Ohnishi, K. Tanie. Accurate Torque Control for a Geared DC Motor based on Acceleration Controller. Proc. of IEEE Int. Conf. on Industrial Electronics Instrumentation and Control, pp. 395-400, San Diego, US, 1992.